Biochemical Journal (2021) **478** 1795–1808
https://doi.org/10.1042/BCJ20210091

PORTLAND PRESS

Research Article

Abiological catalysis by myoglobin mutant with a genetically incorporated unnatural amino acid

Subhash Chand[1,2], Sriparna Ray[1,3], Poonam Yadav[4,*], Susruta Samanta[3], Brad S. Pierce[5] and Roshan Perera[1]

[1]Department of Chemistry and Biochemistry, The University of Texas at Arlington, Arlington, TX, U.S.A.; [2]Department of Anesthesiology, University of Nebraska Medical Center, Omaha, NE 68198, U.S.A.; [3]Department of Chemistry, Manipal University Jaipur, Jaipur, Rajasthan 303007, India; [4]CHI Health, Creighton University Medical Center, Omaha, NE 68124, U.S.A.; [5]Department of Chemistry and Biochemistry, The University of Alabama, Tuscaloosa, AL 35487, U.S.A.

Correspondence: Subhash Chand (subhash.chand@mavs.uta.edu; subhash.ecc@gmail.com)

To inculcate biocatalytic activity in the oxygen-storage protein myoglobin (Mb), a genetically engineered myoglobin mutant H64DOPA (DOPA = L-3,4-dihydroxyphenylalanine) has been created. Incorporation of unnatural amino acids has already demonstrated their ability to accomplish many non-natural functions in proteins efficiently. Herein, the presence of redox-active DOPA residue in the active site of mutant Mb presumably stabilizes the compound I in the catalytic oxidation process by participating in an additional hydrogen bonding (H-bonding) as compared to the WT Mb. Specifically, a general acid-base catalytic pathway was achieved due to the availability of the hydroxyl moieties of DOPA. The reduction potential values of WT ($E° = -260$ mV) and mutant Mb ($E° = -300$ mV), w.r.t. Ag/AgCl reference electrode, in the presence of hydrogen peroxide, indicated an additional H-bonding in the mutant protein, which is responsible for the peroxidase activity of the mutant Mb. We observed that in the presence of 5 mM H_2O_2, H64DOPA Mb oxidizes thioanisole and benzaldehyde with a 10 and 54 folds higher rate, respectively, as opposed to WT Mb. Based on spectroscopic, kinetic, and electrochemical studies, we deduce that DOPA residue, when present within the distal pocket of mutant Mb, alone serves the role of His/Arg-pair of peroxidases.

Introduction

With the aim to mimic the catalytic activity of metalloenzymes in important organic transformations, their rational design and 'repurposing' activities are extremely useful in order to gain a better perspective of these proteins [1–9]. Myoglobin (Mb) is a stable heme-protein that can tolerate multiple mutations near its active site [10–12]. Previously we have genetically modified Mb by incorporating non-canonical amino acid at several positions to attain varied functions [13–15]. At the distal site of Mb, oxygen can directly bind to the heme-iron, while at the axial position, a histidine residue links the heme center to the protein moiety [16]. Various residues present in the vicinity of the active site are critical in determining the catalytic activity and electronic nature of the heme center [13,17,18]. A variety of metalloenzymes (peroxidases, catalases, cytochrome P450s, etc.) oxidize substrates and reduce H_2O_2 while inserting oxygen atom(s) into the substrates [17,19]. Because of its ability to prepare mixed ligand complexes with Fe (ferric, ferrous, and ferryl species) [20], Mb has frequently been used to mimic metalloenzymes [21–26]. Recent studies have implied Mb in various functions such as oxidases, peroxidases, and scavengers [27–31].

The iron-based peroxidases carry out substrate oxidation with H_2O_2 reduction (Scheme 1 Reaction 1) effectively, [9,32] while cytochrome P450s facilitate insertion of a single oxygen atom into different compounds (Scheme 1 Reaction 2) [33,34].

*Voluntary Affiliations.

Received: 12 February 2021
Revised: 1 April 2021
Accepted: 6 April 2021

Accepted Manuscript online: 6 April 2021
Version of Record published: 14 May 2021

Biochemical Journal (2021) **478** 1795–1808
https://doi.org/10.1042/BCJ20210091

Peroxidase	$AH_2 + H_2O_2 \rightarrow A + 2H_2O$	(Reaction 1)
Monooxygenase	$R\text{-}H + O_2 + 2H+ + 2e\text{-} \rightarrow R\text{-}OH + H_2O$	(Reaction 2)

Scheme 1. Reactions of peroxidases and monooxygenase.

Thus, utilizing H_2O_2, peroxidases oxidize the substrates in three consecutive redox steps. First, H_2O_2 oxidizes enzyme, whereby two high-valent Fe (IV) intermediates, namely compound I and compound II, are formed. They oxidize the substrate while reducing back to the native ferric state [35]. As shown in Figure 1A compound I formation in horseradish peroxidase (HRP) occurs by heterolytic cleavage of O-O bond facilitated by His 42. Presence of surrounding residues like Arg 38 and His 42 assists compound I formation and stabilization at the active site of peroxidases (Figure 1B). In wild type Mb, most of the O-O bond cleavage occurs by homolysis, which leads to the formation of compound II (Figure 1C,D). Although heterolytic cleavage has been proposed in Mb for peroxidases activity, the *absence of compound I stabilizing residues at its distal pocket leads to the rapid decay of compound I to compound II* [17,27,29,36]. To incorporate biocatalytic activity by facilitating compound I formation and its stabilization, we have designed an H64DOPA Mb mutant by genetically incorporating an unnatural amino acid, L-3,4-dihydroxyphenylalanine (DOPA), at His 64 position. Being a redox-active amino acid, DOPA is expected to assist in the formation and stabilization of the active intermediate in the catalytic mechanism.

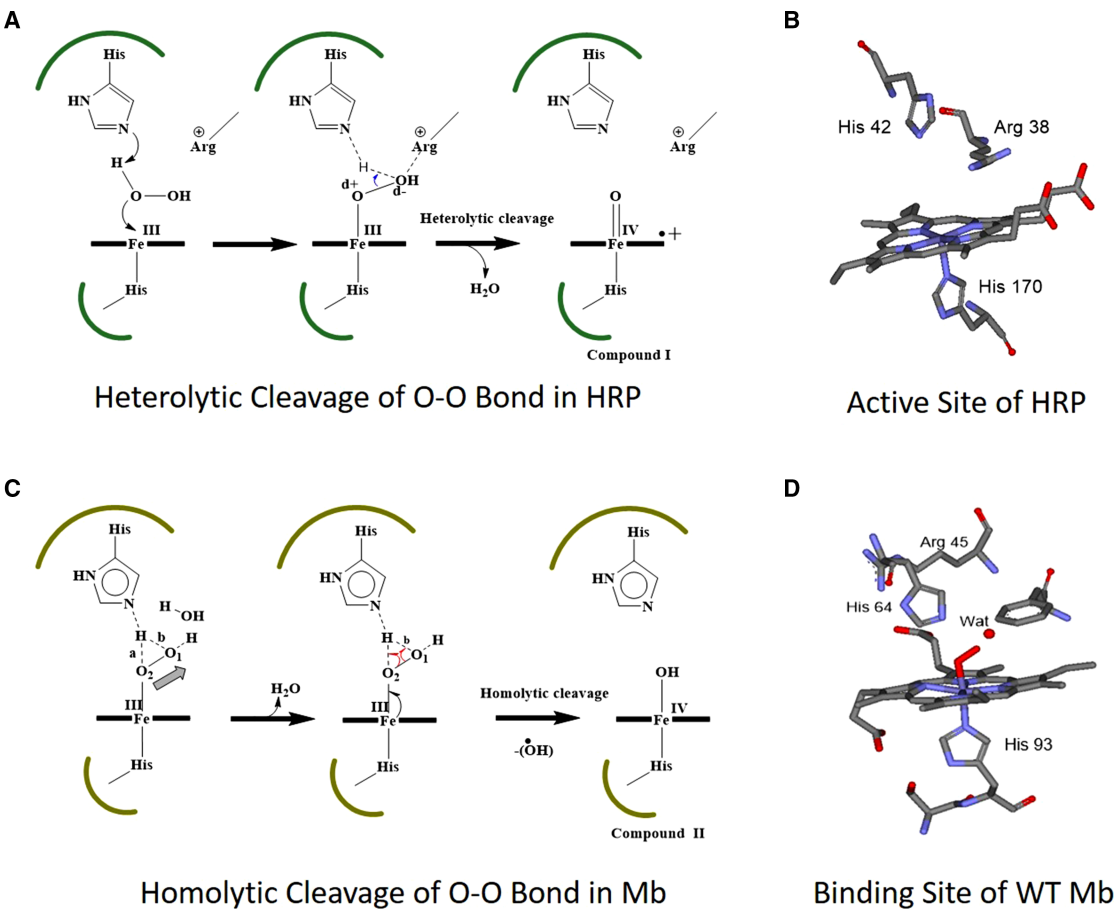

Figure 1. Schematic representation of compound I and compound II formation in HRP and Mb.

(**A**) compound I formation in HRP by heterolytic cleavage; (**B**) Active site of horseradish peroxidase (HRP) (PDB 1HCH); (**C**) Formation of compound II by homolytic cleavage of O-O bond in Mb; (**D**) Binding site of Mb (PDB 1MBO).

Biochemical Journal (2021) **478** 1795–1808
https://doi.org/10.1042/BCJ20210091

Materials and methods

Chemicals

Sodium dithionite, thioanisole, benzaldehyde, 30% hydrogen peroxide, 2,2′-azino-bis (3-ethylbenzothiazoline-6-sulphonic acid) (ABTS), and L-3,4-dihydroxyphenylalanine were purchased from Sigma-Aldrich and used without further purification. All chemicals were of analytical grade or better. The O_2 and N_2 gases were purchased from Air Liquide.

Wild-type Mb and H64DOPA Mb mutant constructs preparation

The WT Mb and H64DOPA Mb constructs were prepared following the previously described method [13–15]. In brief, the WT Mb expression construct and its H64TAG gene were cloned into an ampicillin resistance pBAD expression vector. The aminoacyl tRNA synthetase (aa-tRNA S) plasmid was a generous gift from Prof. Peter Schultz. The H64DOPA Mb expression vector and chloramphenicol resistant tRNA synthetase plasmids were co-transformed in DH10B *E. coli* bacterial cells. The double antibiotic (chloramphenicol and ampicillin) resistant colonies were picked and grown. The glycerol cell stocks were stored at −80°C and used for protein expression.

WT Mb and H64DOPA Mb protein purification

WT Mb and H64DOPA Mb protein were expressed and purified from *E. coli* following the previous protocol [14,15,37]. Briefly, the bacteria were grown in glycerol minimal media with suitable antibiotics, and protein expression was induced by adding arabinose (0.02% w/v) to the bacterial cultures at $O.D_{600}$ 0.5. The proteins were purified by His-Trap Ni-NTA beads and were stored at −80°C until further use.

Protein analysis

The purified proteins were analyzed by SDS-PAGE and matrix-assisted laser desorption/ionization - time-of-flight (MALDI-TOF). The SDS-PAGE analysis showed clean bands for WT and H64DOPA mutant Mb (Supplementary Figure S1). The MALDI-TOF mass spectrometer analysis revealed the mass of 18 397 Da for H64DOPA proteins (Supplementary Figure S2), which is within the accepted margin of error range (±1 Da) of the theoretically-calculated mass (18 398 Da). No wild-type protein (predicted mass, 18 356 ± 1 Da) was observed in the mutant sample, which further accentuates the purity of the protein.

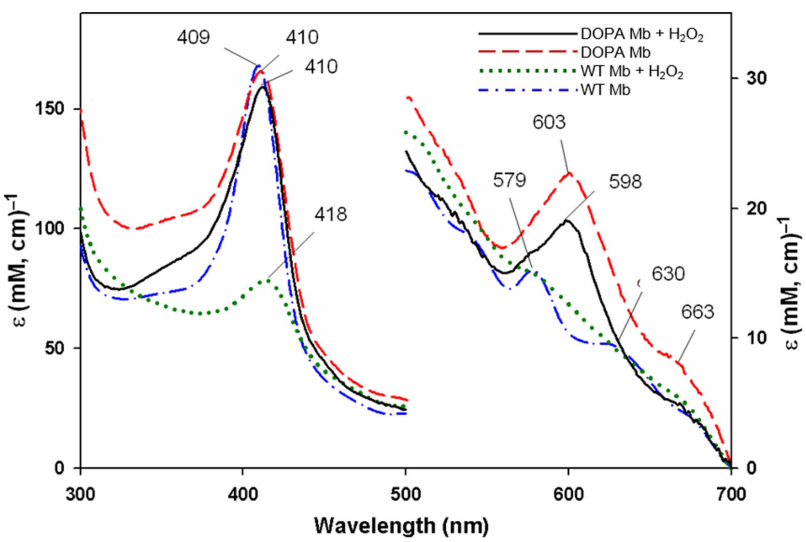

Figure 2. High-valent heme complexes of WT and H64DOPA Mb.

Electronic absorption spectra of the H64DOPA Mb in the presence (solid black line), in the absence (red dashed line) and WT Mb in the presence (green dotted line), and in the absence (blue dashed-dot line) of 5 mM H_2O_2.

Biochemical Journal (2021) 478 1795–1808
https://doi.org/10.1042/BCJ20210091

Spectroscopy

Varian Cary 50 Bio UV-visible spectrophotometer was used to acquire UV-visible electronic absorption spectra of WT and H64DOPA Mb. WT Mb and mutant H64DOPA Mb protein concentrations were calculated from the absorption spectrum, using the molar extinction coefficient value of 170 mM^{-1} cm^{-1} at 409 nm and 411 nm, respectively [13–15]. The effect of hydrogen peroxide on ferric proteins UV-visible electronic absorption spectra was observed in the presence of 5 mM H_2O_2 on 5 μM protein concentration at 20°C (Figure 2). X-band (9 GHz) EPR spectra were recorded on a Bruker EMX Plus spectrometer equipped with a bimodal resonator (Bruker model 4116DM). Low-temperature measurements were made using an Oxford ESR900 cryostat and an Oxford ITC 503 temperature controller. A modulation frequency of 100 kHz was used for all EPR spectra. All data EPR data was collected under non-saturating conditions and simulated as described previsoulsy [13].

ABTS peroxidase assay

In 50 mM potassium phosphate buffer (pH 7.0) 20 mg/ml ABTS stock solution was prepared. Varying concentrations of ABTS (0.02 mM to 2 mM) were used to monitor the reaction. Varian Cary 50 Bio UV-visible spectrophotometer was used to observe the formation of ABTS cation radical in a reaction mixture (containing 1 μM protein, 5 mM H_2O_2, and varied concentrations of ABTS) at 730 nm ($\epsilon_{730} = 3.6 \times 10^4$ M^{-1} cm^{-1}).

Oxyferrous complex preparation

The oxyferrous complexes were prepared in a chest freezer, as described previously [13]. At −35 to −45°C, the protein sample containing 65% glycerol (v/v) was taken in 100 mM potassium phosphate buffer (pH 7.0) and degassed with N_2. Under N_2 atmosphere, pre-cooled O_2 gas was bubbled into deoxyferrous protein species for 60 s, and the UV-visible spectra were recorded (Figure 3).

Thioanisole sulfoxidation and benzaldehyde oxidation

The oxidation reactions were done following the previously reported procedures [13]. In brief, 1 mM substrate (either thioanisole or benzaldehyde) was added to a 2 ml glass bottle containing 5 μM protein (WT or H64DOPA Mb) in 100 mM potassium phosphate buffer (pH 7.0). 5 mM H_2O_2 was added to a final volume of 500 μl to initiate the reaction. After 1 h of incubation, the organic products were extracted in dichloromethane and were analyzed by GC-MS (Supplementary Figures S4, S5).

Electrochemical instrumentation

Electrochemical instrumentation was done following a previously reported procedure [13,14]. At 22°C, differential pulse voltammetry (DPV) was carried out on a CHI720C electrochemical analyzer. A polycrystalline gold electrode was used as a working electrode, a platinum wire as the counter electrode, and Ag/AgCl/3.5 M KCl as a reference electrode. All values were reported concerning the reference electrode (Supplementary Figure S6).

Computational analysis

Quantum mechanical calculations were performed to obtain the optimized structure using the Gaussian 09 program, and visualization was done using the Gaussview 5 program.[1] The initial structure of myoglobin was obtained from the protein data bank, which was solved at a resolution of 1.60 Å (PDB code: 1MBO; URL: https://www.rcsb.org/structure/1mbo). Considering the size of the systems, the structures were optimized using the Hartree Fock theory and STO-3G basis set. Quantum mechanical calculations were performed on three systems with variations in mutations and substrates on myoglobin: (i) DOPA64 and HIS93 without any substrates, (ii) DOPA64 and HIS93 with H_2O_2, and (iii) HIS64 and HIS 93 with O_2 [38].

Results and discussion

DOPA myoglobin mutant as a biocatalyst

The inherent property of Mb is to store and transport oxygen. Hence, WT Mb forms a stable and catalytically inert oxy-complex instead of the catalytically active Compound I. In addition, His 64 is known to stabilize the sixth ligand water molecule through hydrogen bonding [17,20,39]. In this study, His 64 has been replaced by DOPA to incorporate the peroxygenase activity in Mb. The presence of the two hydroxyl groups of DOPA can stabilize the Mb mutant by forming an extra hydrogen bond at its active site. Thus, heterolytic cleavage in the

Biochemical Journal (2021) **478** 1795–1808
https://doi.org/10.1042/BCJ20210091

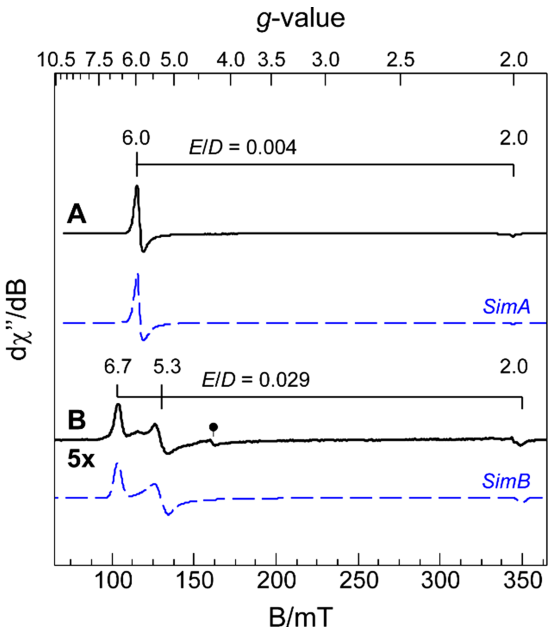

Figure 3. EPR spectroscopic characterization of WT and H64DOPA Fe^{III}-Mb at pH 7.0 A.

X-band EPR spectra (*solid lines*) for wild-type Mb (**A**) and DOPA Mb (**B**) in the resting ferric state at pH 7.0. For clarity, spectra **B** is scaled by 5× for comparison to **A**. Analytical EPR simulations (*dashed lines*) for each are shown below data to determine spectroscopic parameters and determination of spin-concentration. For each (**A** and **B**), the observed EPR spectrum can be fit to a transition within the ground | ±1/2> doublet within an $S = 5/2$ high spin ferric heme. The observed *g*-values for Mb and DOPA-Mb are differentiated only by their rhombicity parameter (*E/D*) [(**A**), 0.004 and (**B**) 0.029]. The feature at $g \sim 4.3$ (●) is attributed to hexaquaFe(III) impurity and accounts for <10 μM. *Simulation parameters*: $D = 13 \pm 3$ cm^{-1}; *E/D*, 0.004 (**A**), 0.0029 (**B**). The intrinsic line width for both **A** and **B** were simulated, assuming a fixed strain in *E/D* ($\sigma_{E/D} \sim 0.005$) and a field distribution (σ_B) matching the instrumental modulation amplitude (0.9 mT). *Instrumental parameters*: microwave frequency, 9.64 GHz; microwave power, 399 μW; modulation amplitude, 0.9 mT; temperature, 10 K.

Fe-hydroperoxo intermediate would be possible, and the catalytic pathway would be facilitated. The genetic incorporation of unnatural amino acids into proteins was done using orthogonal $tRNA_{CUA}$/aminoacyl-tRNA synthetase pairs, as described previously [40]. The mass spectral analysis (MALDI-TOF) revealed a 18 597 Da mass of parent ion as expected for the H64DOPA Mb mutant (18 398 ± 1 Da) (Supplementary Figure S2). In contrast to WT Mb, the H64DOPA Mb mutant showed remarkable tolerance to H_2O_2. Even at 25 mM concentration of H_2O_2, the mutant Mb was tolerant and did not show a significant change in absorbance at 410 nm. When 25 mM H2O2 was added to the WT Mb under similar conditions, it showed a substantial difference in absorbance at 418 nm and was converted to inactive compound II (Supplementary Figure S3).

Characterization of WT and H64DOPA mutant Mb

The mutant and WT Mb exhibited slightly different electronic spectra, as observed for the ferric heme species. The aquo-ferric complex of H64DOPA mutant protein exhibited maximum absorbance Soret at 410 nm and other peaks in the visible region at 603 nm and 663 nm. Aquo-ferric-species of WT Mb showed absorbance Soret at 409 nm and two other peaks (Figure 2). Heme active-site modification with DOPA could account for the slight variation of the mutant spectra. Although the addition of 5 mM H_2O_2 did not show a significant change in spectra ($\lambda_{max} = 410$ and visible peaks at 598 nm and 669 nm) of H64DOPA Mb, there was a definite isosbestic point which indicates the formation of different species. The only slight decrease in the Soret at 410 nm implies that the presence of UAA in the heme pocket had made mutant Mb more tolerant of oxidative degradation, which is more beneficial considering its observed catalytic superiority over WT Mb. In the presence of 5 mM H_2O_2, WT Mb showed similar behavior as previously reported with 409 nm to 418 nm shift in λ_{max} and no other peak in the visible region [13].

Biochemical Journal (2021) **478** 1795–1808
https://doi.org/10.1042/BCJ20210091

EPR spectroscopy was utilized to evaluate perturbations within the DOPA-Mb active site pocket relative to the wild-type Mb protein. As shown in Figure 3, *trace* **A**, the WT Mb exhibited an axial EPR spectrum with effective *g*-values of 6, 6, and 2. This signal arises from the lowest lying Kramers doublet $|m_s = \pm 1/2>$ within the S = 5/2 spin system in axial symmetry ($E/D \sim 0$). Inter-doublet transitions are not observed as the axial zero field splitting (D) is much larger than the incident microwave energy ($D >> hv$). The magnitude of the axial-zero field splitting term was determined by fitting the normalized temperature dependent signal intensity to a Boltzmann population distribution for a three-level system. From this analysis, the value of D was determined to be $+13 \pm 3$ cm^{-1}. Both *g*-values and zero field splitting terms (D and E/D) were consistent with those published previously for high spin WT Mb [13,41,42]. High spin d^5 ions exhibit negligible spin-orbit coupling, therefore all simulations utilize an isotropic *g*-tensor ($g_x = g_y = g_z = 2.00$). Quantitative EPR simulations of spectrum **A** accurately account for 92 ± 5% [413 μM] of iron in the sample assuming near axial symmetry ($E/D = 0.004$).

By contrast, the EPR spectrum observed for the DOPA-Mb variant (Figure 3B) exhibits observed *g*-values of 6.7, 5.3, and 2.0. As with WT Mb, this transition originates from the ground $|m_s = \pm 1/2>$ doublet of a high spin (S = 5/2) ferric heme. However, the effective *g*-values were shifted due to a significant rhombic perturbation ($E/D = 0.029$). Within error, the temperature dependent signal intensity of DOPA-Mb is equivalent to wild-type Mb indicating that these two species have an equivalent axial zero field splitting term (D-value). The sharp transition at $g \sim 4.3$ (●) is attributed to a trace (<5%) impurity from hexaquaFe(III). Since neither of these species contributed significantly to the total iron content, they will not be considered further. A detailed discussion of the structural and electronic factors influencing the zero field splitting rhombicity (E/D) term is presented elsewhere [13]. Distilled down, the increased rhombicity of DOPA-Mb relative to the wild-type suggests that insertion of the non-coordinating DOPA-residue within the outer-sphere distorts the axial solvent ligand away from octahedral symmetry.

Characterization of deoxyferrous and oxyferrous species of WT Mb and H64DOPA Mb

To prepare the oxyferrous complex, the substrate-free low spin ferric form of WT Mb and H64DOPA Mb with 65% (v/v) glycerol were first reduced to ferrous (high spin) form by adding $Na_2S_2O_4$ under N_2 at 4°C. Subsequently, under a nitrogenic atmosphere, pre-cooled O_2 was passed in deoxy-ferrous protein at −35 to −45°C. Deoxyferrous protein showed a shift in the Soret from 409 to 430 nm in WT Mb and from 410 to 432 nm in mutant Mb (Figures 2 and 4). The formation of 430 and 432 Soret bands in WT and H64DOPA Mb is attributed to Fe^{II} -Mb [28,43]. In the visible region, WT Mb deoxyferrous species showed a peak at

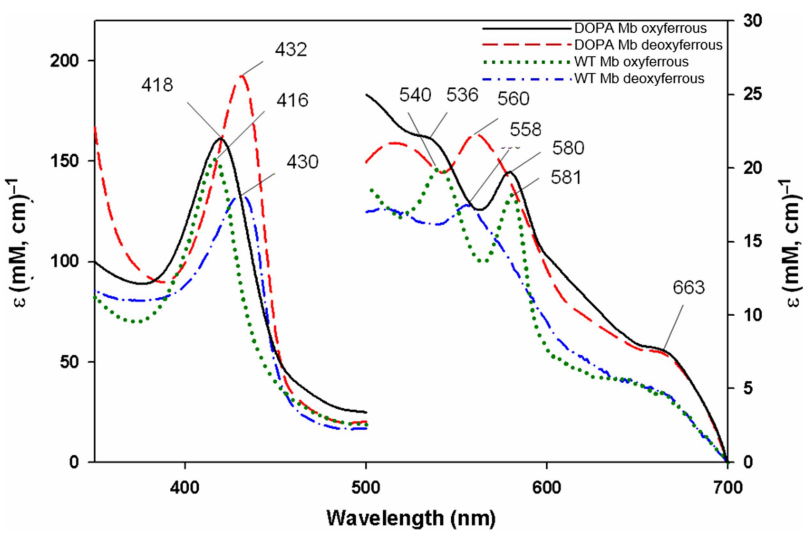

Figure 4. Deoxyferrous and oxyferrous spectra of WT and H64DOPA mutant Mb.

The absorption spectra of WT Mb deoxyferrous (dashed-dot blue line), H64DOPA Mb deoxyferrous (dashed red line), WT Mb oxyferrous (dotted green line), and H64DOPA Mb oxyferrous (solid black line) species. The spectra were taken at −35 to −45°C, and the samples were examined in 65% glycerol, 100 mM phosphate buffer at pH 7.0.

Biochemical Journal (2021) **478** 1795–1808
https://doi.org/10.1042/BCJ20210091

Table 1 Comparison of the UV-visible absorption spectra of WT Mb and H64DOPA Mb derivatives

Mb species	Absorption maxima (nm) in WT Mb	Absorption maxima (nm) in H64DOPA Mb	References
Fe^{III}-Mb	409, 579, 630	410, 603, 663	[1,2], this study
Fe^{II}-Mb	430, 558, 660	432, 505, 560, 663	[1,2], this study
Fe^{II}-O_2-Mb	416, 540, 581	418, 536, 580, 663	[1,2], this study

558 nm, while H64DOPA Mb showed peaks at 560 nm and 515 nm [44], plausibly because DOPA can provide electrons to the heme center and can participate in additional hydrogen bonding. The mutant Mb showed sharper Soret ($\lambda_{max} = 432$) compared to WT Mb (Figures 2 and 4). UV-Vis spectra of the oxy-ferrous complex of WT Mb ($\lambda_{max} = 416$ nm and two visible peaks at 540 nm and 581 nm) were similar to H64DOPA Mb spectra ($\lambda_{max} = 418$ nm and two peaks at 536 nm and 580 nm in the visible region) (Table 1). The subtle differences between WT and mutant Mb spectra could be attributed to the presence of bulkier residue (DOPA) compared to histidine within hydrogen-bonding distance of the heme center.

Electrochemical characterization of WT and mutant H64DOPA Mb

To understand electron and proton transfer mechanism through hydroxyl groups of DOPA in the catalytically active species formation, we probed the mutant and WT Mb protein solutions for their reduction potential (E) using DPV in the presence and absence of H_2O_2 (Supplementary Figure S6). The E values of these proteins indicate that hydroxyl groups of DOPA residue in mutant protein dictate the electronic nature of the iron heme center. In the presence of H_2O_2, the E values were lower both in WT and mutant Mb as H_2O_2 was bonded to the heme center [45]. Binding of H_2O_2 to the heme center replaced the H_2O molecule, the sixth ligand, and a high spin ferric state was formed. The reduction in E value also reduced the energy barrier for electron transfer to the heme center [33,45]. Although in the absence of H_2O_2, both WT and mutant proteins showed the same E value (−232 mV) while in the presence of H_2O_2, the mutant (−300 mV) exhibited a 40 mV shift from WT Mb (−260 mV) (Supplementary Figure S6 and Table 2). The difference in E value of WT and mutant Mb is most likely due to deprotonation of the hydroxyl (-OH) groups of DOPA residue, which also affect the electronic nature of the heme iron center similar to what we have reported earlier [13]. This change of 40 mV is consistent with the fact that the presence of an extra hydrogen bond in H64DOPA (one hydrogen bond changes reduction potential 30–40 mV) would favorably facilitate and stabilize the formation of compound I in the mutant Mb compare to WT Mb [34,46,47] (see Table 2). Hence, electrochemical studies provide substantial evidence that incorporating the DOPA residue in place of His 64 helps attain a similar electrochemical environment at the active site of the modified protein as provided by the His/Arg residue pair in the peroxidase enzymes.

Thioanisole sulfoxidation and benzaldehyde oxidation

Furthermore, to prove the catalytic property of the modified enzyme, two different abiological reactions were identified. Thioanisole sulfoxidation and benzaldehyde oxidation were carried out and compared with WT Mb. In the presence of 5 mM H_2O_2, mutant Mb showed turnover rates of 2.5 ± 0.18 min^{-1} and 2.67 ± 0.24 min^{-1}

Table 2 Reduction potential of WT Mb and H64DOPA Mb mutant at pH 7.0 in the presence and absence of H_2O_2 as obtained from DPV

	Reduction Potential, *E* (V) at pH 7	
Protein	Without H_2O_2	With 5 mM H_2O_2
WT Mb	−0.232	−0.260
H64DOPA Mb	−0.232	−0.300

All protein concentrations were 5 μM, and the potentials were recorded *vs*. Ag/AgCl (3.5 M KCl).

Biochemical Journal (2021) **478** 1795–1808
https://doi.org/10.1042/BCJ20210091

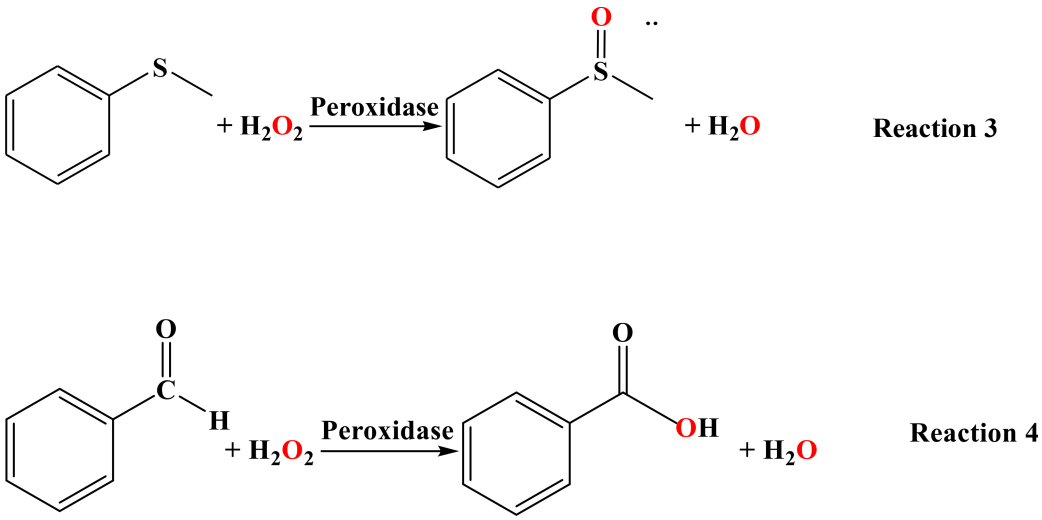

Scheme 2. Oxidation reactions of thioanisole and benzaldehyde.

for thioanisole sulfoxidation (Scheme 2, Reaction 3) and benzaldehyde oxidation (Scheme 2, Reaction 4), respectively. While turnover rates of WT Mb were 0.25 ± 0.02 min^{-1} for sulfoxidation and 0.05 ± 0.004 min^{-1} for benzaldehyde oxidation. Overall, mutant Mb showed 10 and ∼54-folds higher catalytic activity of thioanisole sulfoxidation and benzaldehyde oxidation, respectively, than WT Mb (Table 3).

As shown in Scheme 3, on WT Mb reaction with H_2O_2, the majority of O-O bond goes through homolytic cleavage and forms compound II. Only a trace amount of it follows heterolytic cleavage to form compound I [36]. Compound I is a rather unstable species and immediately decays to compound II, making WT Mb catalytically less active and compound I characterization more challenging [48]. Recently, Rittle and Green could spectroscopically characterize compound I in CYP 119 [49]. In our observations, the mutant H64DOPA Mb was more tolerant to oxidative degradation of H_2O_2 and did not show a significant variation in the absorbance spectrum after the addition of H_2O_2 (Supplementary Figure S3). Presumably, in the mutant Mb, the majority of compound I formed from heterolysis convert back to its ferric state instead of decaying to compound II as in WT Mb (Scheme 3), making mutant Mb catalytically efficient (Table 3) as well as hydrogen peroxide tolerant (Supplementary Figure S3).

Previously Watanabe group had used thioanisole as a substrate for catalytic oxidation. They compared the catalytic activity of F43H/H64L Mb and L29H/H64L (double mutants) with WT Mb [26,50]. In contrast to the WT Mb, both mutants were a superior catalyst; notably, the F43H/H64L mutant Mb showed 200-fold higher thioanisole oxidation. A robust hydrogen-bonding network in F43H/H64L mutant Mb was accredited for the superior catalytic activity of F43H/H64L as compared to both WT Mb and L29H/H64L mutant Mb. A similar character is exhibited by our previously studied $H64NH_2Tyr$ mutant Mb and the present mutant H64DOPA Mb [13]. Under marginally different reaction conditions (50 mM sodium acetate buffer, pH 5.3, at 5.0°C), thioanisole oxidation by H64A Mb and H64S Mb mutants have also been reported with rate constants 1.5×10^6 M^{-1} s^{-1} [36,51]. Recently, Yin et al. [8] reported that in F43Y/H64D Mb mutant, the distal Asp 64

Table 3 Rate of thioanisole sulfoxidation (Reaction 3) and benzaldehyde oxidation (Reaction 4) by WT and H64DOPA mutant Mb

	Rates (min^{-1})	
Protein	**Rxn 3**	**Rxn 4**
WT Mb	0.25 ± 0.02	0.05 ± 0.004
H64DOPA Mb	2.5 ± 0.18	2.67 ± 0.24

Biochemical Journal (2021) 478 1795–1808
https://doi.org/10.1042/BCJ20210091

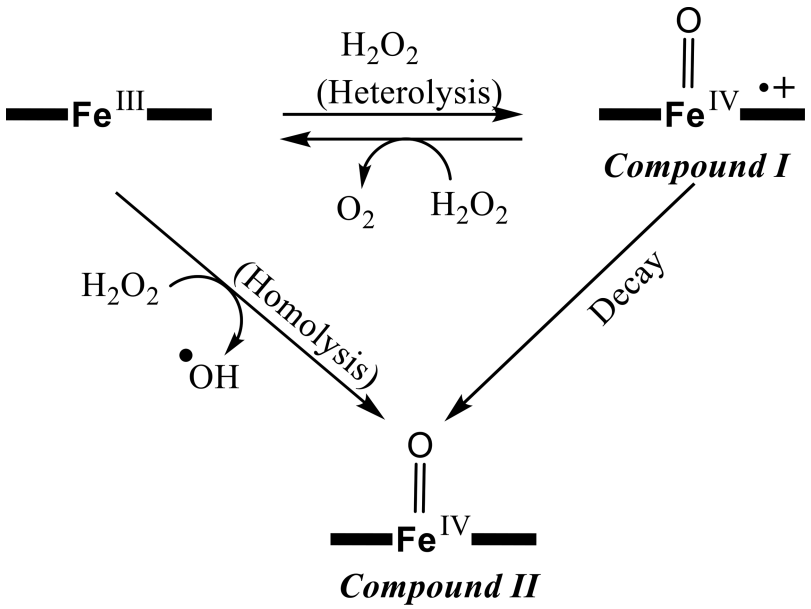

Scheme 3. Plausible reaction scheme of mutant and wild type ferric Mb with hydrogen peroxide.

stabilized enzyme-substrate complex by H-bonding, and mutant Mb was 1000-fold more efficient than native dehaloperoxidase.

ABTS peroxidase assay

2,2′-Azino-bis (3-ethylbenzothiazoline-6-sulphonic acid) (ABTS) has often been used to estimate the reaction kinetics of enzymes like peroxidases [52]. In the presence of H_2O_2 and peroxidase, ABTS gets converted to its radical cation. This blue colored cation radical has been utilized indirectly to identify the formation of the ferryl radical species in peroxidases [36,53]. Hence, the ABTS peroxidase assay was performed in the presence of 5 mM H_2O_2, 1 μM protein, and varying concentrations (0.02 mM to 2 mM) of ABTS to detect the formation of active species both in the WT and mutant H64DOPA Mb at pH 7.0 and 4°C. Formation of ABTS cation radical was monitored at 730 nm, and based on obtained data K_M and k_{cat} (V_{max}/[E]) were calculated using Lineweaver–Burk plots [54]. k_{cat} of WT and mutant H64DOPA Mb were observed to be 24.7 and 15.2 μM min^{-1}, respectively (Table 4).

H64DOPA mutant Mb displayed a K_M of 6.7×10^2 μM, which was ~35 times greater than K_M value of WT Mb. In comparison to WT Mb, the increase in K_M of mutant Mb further indicate that the substrate-binding ability at the active site has been significantly increased due to the incorporation of the non-canonical amino acid in the H64DOPA Mb. Although k_{cat} values of WT and mutant Mb were not reflective of catalytic efficiency, never the less, ABTS peroxidase assay implied the formation of active compound both in WT Mb and in mutant H64DOPA Mb.

Table 4 Peroxidase assay of WT and H64DOPA mutant Mb with ABTS in the presence of H_2O_2[1]

Protein	K_M (μM)	$k_{cat} = v0/[E]$ (min^{-1}) V_{max} (μM min^{-1})
WT Mb	20.4 ± 1.57[2]	24.7 ± 2.23[2]
H64DOPA Mb	$6.7 \pm 0.34 \times 10^2$	15.2 ± 0.91

[1]ABTS oxidation reaction with WT Mb and its H64DOPA mutant Mb carried out in the presence of 5 mM H_2O_2. Kinetic values are based on the average of at least three determinations, and the unit for the rate is turnover per min. The reactions were carried out at pH 7.0 and 4°C;
[2]These values agree with previous reports [1,3].

Biochemical Journal (2021) **478** 1795–1808
https://doi.org/10.1042/BCJ20210091

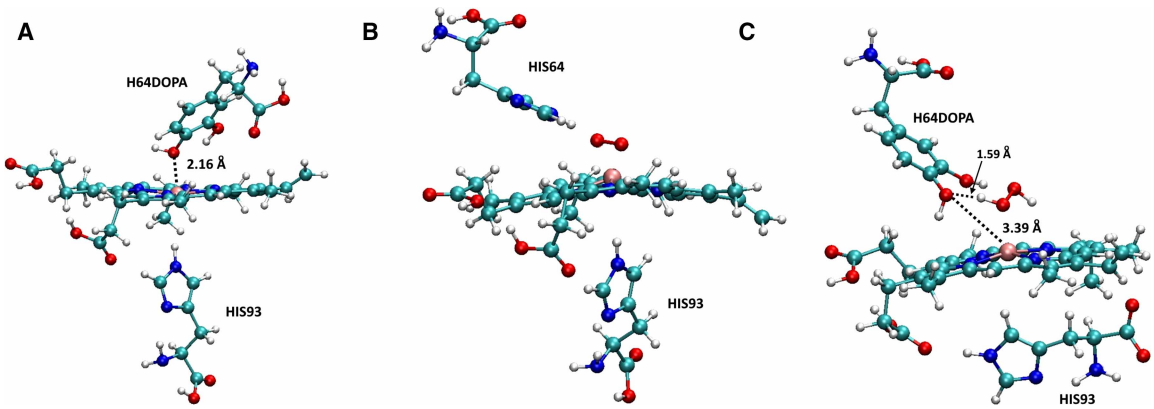

Figure 5. Computational analysis of the active sites of WT Mb and H64DOPA mutant Mb.

(**A**) Structural analysis of active site of mutant H64DOPA Mb: Distance between HIS93 and Fe is 2.75 Å; Distance between DOPA and Fe is 2.16 Å. (**B**) Structural analysis of the WT Mb: Distance between HIS93 and Fe is 2.91 Å; Distance between HIS64 and Fe is 2.16 Å (The structure includes an Oxygen molecule.). (**C**) Structural analysis of active site of mutant H64DOPA Mb: Distance between HIS93 and Fe is 2.84 Å; Distance between DOPA and Fe is 3.39 Å (The structure includes a hydrogen peroxide molecule.); Distance between O of DOPA and H of H_2O_2 1.59 Å.

Computational analysis of Mb mutant's active site

To verify the structural position of DOPA residue within the active site of the mutant H64DOPA Mb, computational analysis of the active site with and without H_2O_2 was carried out (Figure 5). The structural analysis

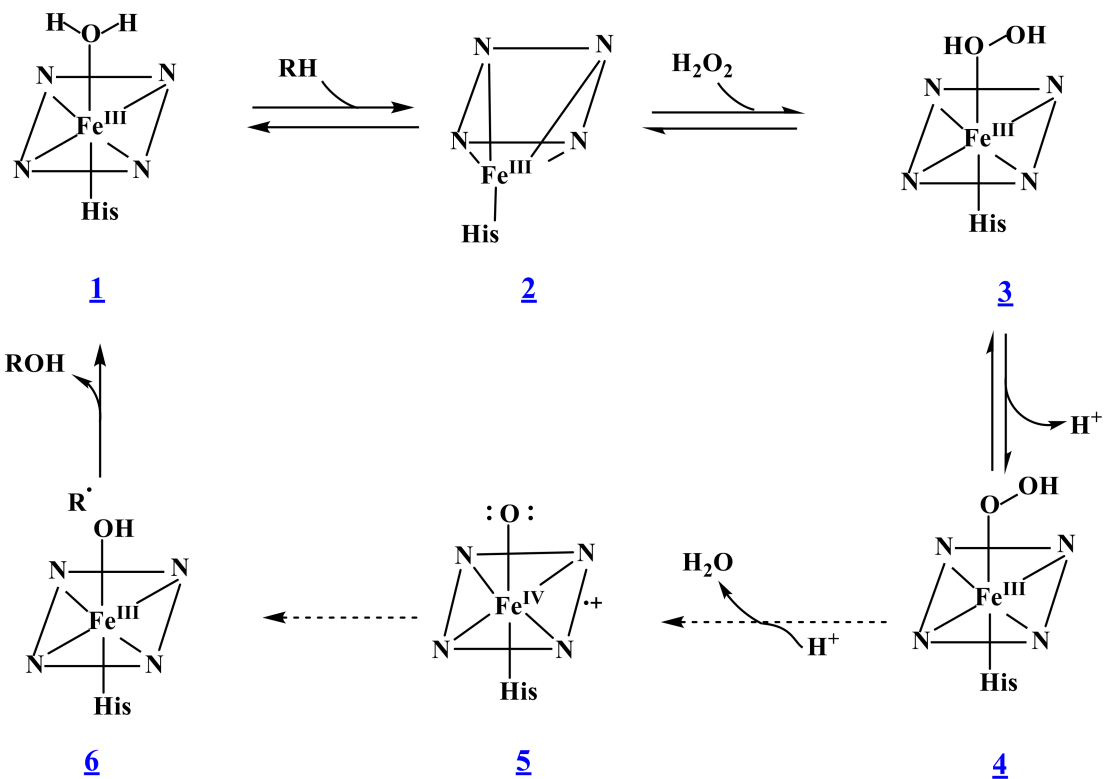

Scheme 4. Formation of compound I in peroxidase shunt pathway.

1: ferric low-spin (S = 1/2); **2**: ferrous high-spin (S = 5/2); **3**: Fe^{+3} (H_2O_2) intermediate; **4**: ferric-hydroperoxo intermediate (Compound 0); **5**: highly reactive porphyrin π radical cation (compound I); **6**: Compound II and substrate radical.

Biochemical Journal (2021) **478** 1795–1808
https://doi.org/10.1042/BCJ20210091

revealed that in the absence of H_2O_2, the distance between the DOPA residue and the Fe center (2.16 Å) was comparable with the His64 and Fe center (2.16 Å). But in the presence of H_2O_2, the active site of the mutant was altered considerably. Due to the interaction of H_2O_2 molecule and the DOPA residue, the distance between DOPA and the Fe center is increased to 3.39 Å. This would easily enable the entry and oxidation of various organic substrates in the mutant H64DOPA Mb, which was not observed in WT Mb. In addition, the distance between the oxygen atom in DOPA and one of the H-atom of H_2O_2 is 1.59 Å, which is within the range of hydrogen bonding between oxygen and hydrogen atoms.

Mechanistic insinuations of Mb mutant's activity

Although a detailed investigation of the catalytic mechanism was not feasible within the extent of this study, some insight could be drawn and utilized for future studies. To explain the observed catalytic reactions, the formation of compound I like species would be essential, which enabled the catalytic oxidation of the substrate. General acid-base catalysis proposed earlier [13] can enable this catalytic reaction. Peroxidase shunt pathway begins with the binding of substrate to water-coordinated low-spin (S = 1/2) ferric enzyme (resting-state **1**) (Scheme 4). Substrate binding displaces water as the sixth ligand and forms pentacoordinate high spin (S = 5/2) enzyme-substrate adduct **2**. Following this, there is a shift in the heme's redox potential from −330 to −173 mV [45]. Addition of H_2O_2 changes it to a Fe^{+3} (H_2O_2) intermediate **3**. Deprotonation of this intermediate leads to the ferric-hydroperoxo intermediate, known as compound 0 **4**. Protonation of compound 0 leads to heterolytic cleavage of O-O bond forming compound I **5**, a porphyrin π radical cation ferryl complex.

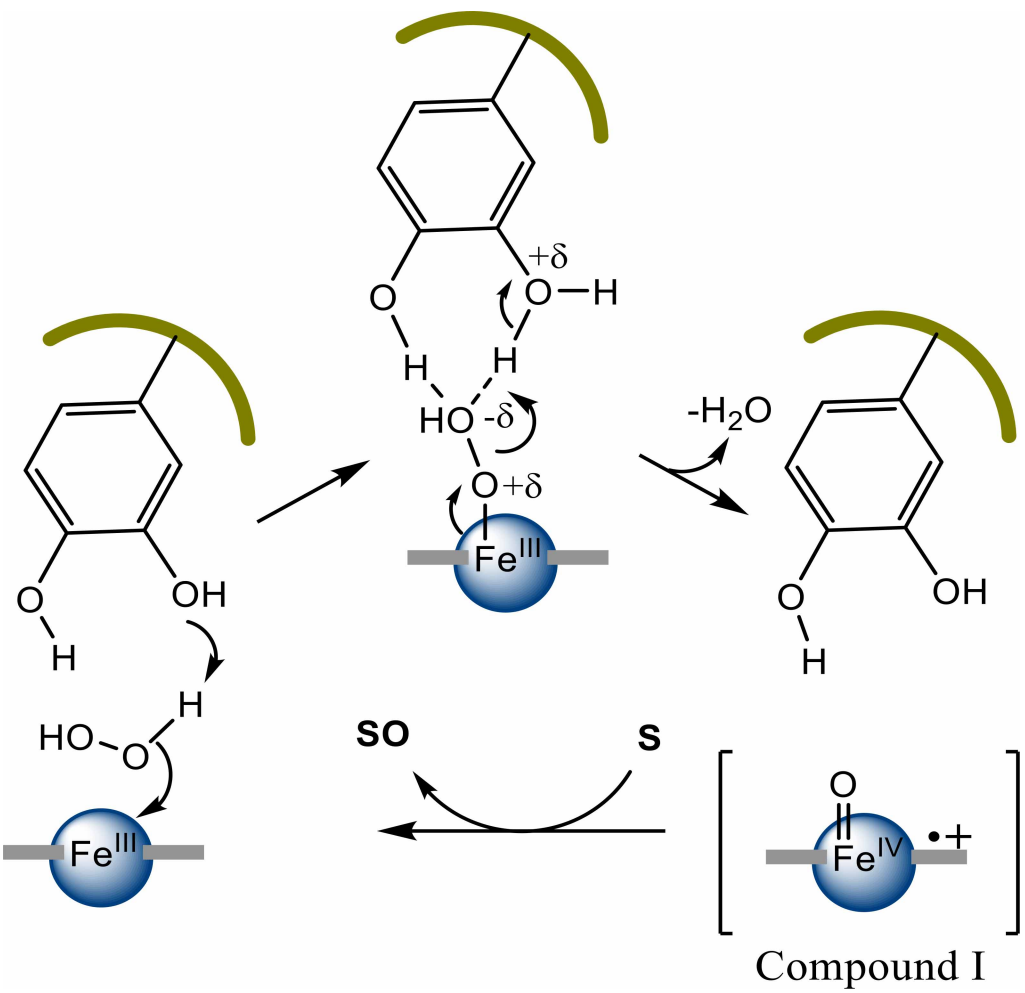

Scheme 5. Plausible role of the redox-active DOPA in compound I formation and substrate oxidation.

Biochemical Journal (2021) **478** 1795–1808
https://doi.org/10.1042/BCJ20210091

Compound I abstracts an H atom from the substrate, leading to ferryl hydroxyl intermediate (also known as Compound II) and a substrate radical **6**. The hydroxyl moiety on heme iron binds with the substrate radical to form the oxidative product, and the enzyme returns to its resting state **1** [34,47].

The hydroxyl groups of the DOPA facilitate the mechanism (Scheme 5) as they can interact and form a hydrogen bond with H_2O_2. This was also confirmed through the computational analysis of the active site in the presence of H_2O_2. Consequently, a Fe-O-OH moiety (Compound **0**) can form and heterolytic cleavage of the O-O bond produces the active ferryl radical cation (Compound I). Thus, the extra hydrogen bond appears to be instrumental in the formation and stabilization of the compound I species in the mutant H64DOPA Mb, thereby enhancing the catalytic oxidation of both thioanisole and benzaldehyde.

Conclusion

In this study, we report incorporating an unnatural amino acid (L-DOPA) in a specific position within the binding site of Mb. Mutant H64DOPA Mb is an active and stable protein which in the presence of hydrogen peroxide, can catalyze abiological reactions, such as thioanisole sulfoxidation and benzaldehyde oxidation with 10 to 54 folds higher catalytic rate than WT Mb. Our findings indicate that the redox properties of DOPA can be exploited to 'repurpose' a metalloprotein and incorporate catalytic activity in mutant H64DOPA Mb.

Additionally, our observations support that the distal residues at the heme active site are critical for compound I formation and stability. To exhibit peroxygenase activity in Mb, the mutation of the distal His with the unnatural amino acid, L-DOPA, assisted in substrate binding at the active site and enhanced its ability to oxidize small organic molecules. Such abiological transformations carried out by modified metalloproteins can be utilized by the pharmaceutical industries for various biocatalytic applications. Avoiding chemical catalysts can help us achieve the different green principles of chemical reactions, like 'less hazardous chemical synthesis' or 'use of enzymatic catalysts, instead of stoichiometric reagents.' In our study, the mutant H64DOPA Mb efficiently exhibited that abiological substrates can be used, and the mutant Mb can achieve the peroxidase-type activity. Such 'repurposed metalloproteins' can be utilized in similar abiological reactions instead of chemical catalysts. In this regard, it is noteworthy that myoglobin's robustness is essential to modify it for efficient 'repurposing' activities. We observed that mutant H64DOPA Mb is tolerant towards a higher concentration of H_2O_2, which considerably proves its robustness and its abiological catalytic applicability. Thus, our aim to modify the active site of Mb through rational design and 'repurpose' the metalloprotein was successful as mutant H64DOPA Mb catalyzed the monoxidation of thioanisole and benzaldehyde.

Data Availability

All data that support the findings of this study are contained within the main article and its Supplementary Files.

Competing Interests

The authors declare that there are no competing interests associated with the manuscript.

Funding

This study was supported by the Department of Chemistry and Biochemistry, The University of Texas, Arlington, TX, USA. This work was also supported by grants from the National Institutes of Health (2 R15 GM117511-01 to B.S.P.) and the National Science Foundation (CHE, 1709369 to B.S.P).

CRediT Author Contribution

Subhash Chand: Conceptualization, Data curation, Formal analysis, Validation, Investigation, Methodology, Writing — original draft, Project administration, Writing — review and editing. **Sriparna Ray:** Conceptualization, Formal analysis, Investigation, Writing — review and editing. **Poonam Yadav:** Writing — review and editing. **Susruta Samanta:** Software, Formal analysis, Investigation, Writing — review and editing. **Brad S. Pierce:** Software, Formal analysis, Investigation, Writing — review and editing. **Roshan Perera:** Conceptualization, Supervision, Writing — review and editing.

Acknowledgements

We thank Professor Peter G. Schultz for his generous gift of the tRNA-synthetase system and Professor Krishnan Rajeshwar for many productive discussions. We also thank Professor Daniel W. Armstrong for letting

us use his lab facilities for the GC-MS analysis. We are grateful to Joshua Crawford for assisting in EPR experiments.

Abbreviations

ABTS, 2,2′-azino-bis (3-ethylbenzothiazoline-6-sulphonic acid); DOPA, L-3,4-dihydroxyphenylalanine
DPV, differential pulse voltammetry; HRP, horseradish peroxidase; MALDI-TOF, matrix-assisted laser desorption/ionization - time-of-flight.

References

1 Yu, Y., Cui, C., Liu, X., Petrik, I.D., Wang, J. and Lu, Y. (2015) A designed metalloenzyme achieving the catalytic rate of a native enzyme. *J. Am. Chem. Soc.* **137**, 11570–11573 https://doi.org/10.1021/jacs.5b07119
2 Hyster, T.K. and Ward, T.R. (2016) Genetic optimization of metalloenzymes: enhancing enzymes for non-natural reactions. *Angew. Chem. Int. Ed. Engl.* **55**, 7344–7357 https://doi.org/10.1002/anie.201508816
3 Shu, X.G., Su, J.H., Du, K.J., You, Y., Gao, S.Q., Wen, G.B. et al. (2016) Rational design of dual active sites in a single protein scaffold: a case study of heme protein in myoglobin. *ChemistryOpen* **5**, 192–196 https://doi.org/10.1002/open.201500224
4 Oohora, K. and Hayashi, T. (2014) Hemoprotein-based supramolecular assembling systems. *Curr. Opin. Chem. Biol.* **19**, 154–161 https://doi.org/10.1016/j.cbpa.2014.02.014
5 Yeung, N., Lin, Y.W., Gao, Y.G., Zhao, X., Russell, B.S., Lei, L. et al. (2009) Rational design of a structural and functional nitric oxide reductase. *Nature* **462**, 1079–1082 https://doi.org/10.1038/nature08620
6 Brandenberg, O.F., Fasan, R. and Arnold, F.H. (2017) Exploiting and engineering hemoproteins for abiological carbene and nitrene transfer reactions. *Curr. Opin. Biotechnol.* **47**, 102–111 https://doi.org/10.1016/j.copbio.2017.06.005
7 Shoji, O. and Watanabe, Y. (2014) Peroxygenase reactions catalyzed by cytochromes P450. *J. Biol. Inorg. Chem.* **19**, 529–539 https://doi.org/10.1007/s00775-014-1106-9
8 Yin, L.L., Yuan, H., Liu, C., He, B., Gao, S.-Q., Wen, G.-B. et al. (2018) A rationally designed myoglobin exhibits a catalytic dehalogenation efficiency more than 1000-fold that of a native dehaloperoxidase. *ACS Catalysis* **8**, 9619–9624 https://doi.org/10.1021/acscatal.8b02979
9 Lucic, M., Chaplin, A.K., Moreno-Chicano, T., Dworkowski, F.S.N., Wilson, M.T., Svistunenko, D.A. et al. (2020) A subtle structural change in the distal haem pocket has a remarkable effect on tuning hydrogen peroxide reactivity in dye decolourising peroxidases from Streptomyces lividans. *Dalton Trans.* **49**, 1620–1636 https://doi.org/10.1039/C9DT04583J
10 Ordway, G.A. and Garry, D.J. (2004) Myoglobin: an essential hemoprotein in striated muscle. *J. Exp. Biol.* **207**, 3441–3446 https://doi.org/10.1242/jeb.01172
11 Kendrew, J.C. (1963) Myoglobin and the structure of proteins. *Science* **139**, 1259–1266 https://doi.org/10.1126/science.139.3561.1259
12 Hargrove, M.S., Krzywda, S., Wilkinson, A.J., Dou, Y., Ikeda-Saito, M. and Olson, J.S. (1994) Stability of myoglobin: a model for the folding of heme proteins. *Biochemistry* **33**, 11767–11775 https://doi.org/10.1021/bi00205a012
13 Chand, S., Ray, S., Wanigasekara, E., Yadav, P., Crawford, J.A., Armstrong, D.W. et al. (2017) Improved rate of substrate oxidation catalyzed by genetically-engineered myoglobin. *Arch. Biochem. Biophys.* **639**, 44–51 https://doi.org/10.1016/j.abb.2017.12.014
14 Ray, S., Chand, S., Zhang, Y.B., Nussbaum, S., Rajeshwar, K. and Perera, R. (2013) Implications of active site orientation in myoglobin for direct electron transfer and electrocatalysis based on monolayer and multilayer covalent immobilization on gold electrodes. *Electrochim. Acta* **99**, 85–93 https://doi.org/10.1016/j.electacta.2013.03.080
15 Stamos, B., Loredo, L., Chand, S., Phan, T.V., Zhang, Y., Mohapatra, S. et al. (2012) Biosynthetic approach for functional protein microarrays. *Anal. Biochem.* **424**, 114–123 https://doi.org/10.1016/j.ab.2012.02.019
16 Phillips, S.E. (1980) Structure and refinement of oxymyoglobin at 1.6 A resolution. *J. Mol. Biol.* **142**, 531–554 https://doi.org/10.1016/0022-2836(80)90262-4
17 Matsui, T., Ozaki, S., Liong, E., Phillips, Jr, G.N. and Watanabe, Y. (1999) Effects of the location of distal histidine in the reaction of myoglobin with hydrogen peroxide. *J. Biol. Chem.* **274**, 2838–2844 https://doi.org/10.1074/jbc.274.5.2838
18 Hara, I., Ueno, T., Ozaki, S., Itoh, S., Lee, K., Ueyama, N. et al. (2001) Oxidative modification of tryptophan 43 in the heme vicinity of the F43W/H64L myoglobin mutant. *J. Biol. Chem.* **276**, 36067–36070 https://doi.org/10.1074/jbc.C100371200
19 Takano, T. (1977) Structure of myoglobin refined at 2-0 A resolution. II. Structure of deoxymyoglobin from sperm whale. *J. Mol. Biol.* **110**, 569–584 https://doi.org/10.1016/S0022-2836(77)80112-5
20 Phillips, Jr, G.N., Arduini, R.M., Springer, B.A. and Sligar, S.G. (1990) Crystal structure of myoglobin from a synthetic gene. *Proteins* **7**, 358–365 https://doi.org/10.1002/prot.340070407
21 Ozaki, S., Matsui, T., Roach, M.P. and Watanabe, Y. (2000) Rational molecular design of a catalytic site: engineering of catalytic functions to the myoglobin active site framework. *Coord. Chem. Rev.* **198**, 39–59 https://doi.org/10.1016/S0010-8545(00)00234-4
22 Yang, H.J., Matsui, T., Ozaki, S., Kato, S., Ueno, T., Phillips, Jr, G.N. et al. (2003) Molecular engineering of myoglobin: influence of residue 68 on the rate and the enantioselectivity of oxidation reactions catalyzed by H64D/V68X myoglobin. *Biochemistry* **42**, 10174–10181 https://doi.org/10.1021/bi034605u
23 Pfister, T.D., Ohki, T., Ueno, T., Hara, I., Adachi, S., Makino, Y. et al. (2005) Monooxygenation of an aromatic ring by F43W/H64D/V68I myoglobin mutant and hydrogen peroxide. Myoglobin mutants as a model for P450 hydroxylation chemistry. *J. Biol. Chem.* **280**, 12858–12866 https://doi.org/10.1074/jbc.M410853200
24 Du, J., Sono, M. and Dawson, J.H. (2011) The H93G myoglobin cavity mutant as a versatile scaffold for modeling heme iron coordination structures in protein active sites and their characterization with magnetic circular dichroism spectroscopy. *Coord. Chem. Rev.* **255**, 700–716 https://doi.org/10.1016/j.ccr.2011.01.029
25 Tyagi, V. and Fasan, R. (2016) Myoglobin-catalyzed olefination of aldehydes. *Angew. Chem. Int. Ed. Engl.* **55**, 2512–2516 https://doi.org/10.1002/anie.201508817

Biochemical Journal (2021) **478** 1795–1808
https://doi.org/10.1042/BCJ20210091

26 Ozaki, S.I., Matsui, T. and Watanabe, Y. (1996) Conversion of myoglobin into a highly stereospecific peroxygenase by the L29H/H64L mutation. *J. Am. Chem. Soc.* **118**, 9784–9785 https://doi.org/10.1021/ja961223l

27 Jia, H.-Y., Zong, M.-H., Zheng, G.-W. and Li, N. (2019) Myoglobin-catalyzed efficient in situ regeneration of NAD(P)+ and their synthetic biomimetic for dehydrogenase-mediated oxidations. *ACS Catalysis* **9**, 2196–2202 https://doi.org/10.1021/acscatal.8b04890

28 Bostelaar, T., Vitvitsky, V., Kumutima, J., Lewis, B.E., Yadav, P.K., Brunold, T.C. et al. (2016) Hydrogen sulfide oxidation by myoglobin. *J. Am. Chem. Soc.* **138**, 8476–8488 https://doi.org/10.1021/jacs.6b03456

29 Mannino, M.H., Patel, R.S., Eccardt, A.M., Perez Magnelli, R.A., Robinson, C.L.C., Janowiak, B.E. et al. (2019) Myoglobin as a versatile peroxidase: implications for a more important role for vertebrate striated muscle in antioxidant defense. *Comp. Biochem. Physiol. B Biochem. Mol. Biol.* **234**, 9–17 https://doi.org/10.1016/j.cbpb.2019.04.005

30 Zhang, P., Yuan, H., Xu, J., Wang, X.-J., Gao, S.-Q., Tan, X. et al. (2020) A catalytic binding site together with a distal Tyr in myoglobin affords catalytic efficiencies similar to natural peroxidases. *ACS Catalysis* **10**, 891–896 https://doi.org/10.1021/acscatal.9b05080

31 Ascenzi, P., De Simone, G., Tundo, G.R., Platas-Iglesias, C. and Coletta, M. (2020) Ferric nitrosylated myoglobin catalyzes peroxynitrite scavenging. *J. Biol. Inorg. Chem.* **25**, 361–370 https://doi.org/10.1007/s00775-020-01767-2

32 Wang, Y., Lan, D., Durrani, R. and Hollmann, F. (2017) Peroxygenases en route to becoming dream catalysts. What are the opportunities and challenges? *Curr. Opin. Chem. Biol.* **37**, 1–9 https://doi.org/10.1016/j.cbpa.2016.10.007

33 Dawson, J.H. (1988) Probing structure-function relations in heme-containing oxygenases and peroxidases. *Science* **240**, 433–439 https://doi.org/10.1126/science.3358128

34 Unno, M., Shimada, H., Toba, Y., Makino, R. and Ishimura, Y. (1996) Role of Arg112 of cytochrome p450cam in the electron transfer from reduced putidaredoxin. Analyses with site-directed mutants. *J. Biol. Chem.* **271**, 17869–17874 https://doi.org/10.1074/jbc.271.30.17869

35 Azevedo, A.M., Martins, V.C., Prazeres, D.M., Vojinovic, V., Cabral, J.M. and Fonseca, L.P. (2003) Horseradish peroxidase: a valuable tool in biotechnology. *Biotechnol. Annu. Rev.* **9**, 199–247 https://doi.org/10.1016/S1387-2656(03)09003-3

36 Matsui, T., Ozaki, S. and Watanabe, Y. (1999) Formation and catalytic roles of compound I in the hydrogen peroxide-dependent oxidations by His64 myoglobin mutants. *J. Am. Chem. Soc.* **121**, 9952–9957 https://doi.org/10.1021/ja9914846

37 Chand, S., Messina, E.L., AlSalmi, W., Ananthaswamy, N., Gao, G., Uritskiy, G. et al. (2017) Glycosylation and oligomeric state of envelope protein might influence HIV-1 virion capture by alpha4beta7 integrin. *Virology* **508**, 199–212 https://doi.org/10.1016/j.virol.2017.05.016

38 Frisch, M.J., Trucks, G.W., Schlegel, H.B., Scuseria, G.E., Robb, M.A., Cheeseman, J.R. et al. (2016) *Gaussian 16 Rev. C.01*, Gaussian Inc, Wallingford, CT

39 Takano, T. (1977) Structure of myoglobin refined at 2-0 A resolution. I. Crystallographic refinement of metmyoglobin from sperm whale. *J. Mol. Biol.* **110**, 537–568 https://doi.org/10.1016/S0022-2836(77)80111-3

40 Young, T.S. and Schultz, P.G. (2010) Beyond the canonical 20 amino acids: expanding the genetic lexicon. *J. Biol. Chem.* **285**, 11039–11044 https://doi.org/10.1074/jbc.R109.091306

41 Kao, Y.H. and Lecomte, J.T.J. (1993) Determination of the zero-field splitting constant for proton NMR chemical shift analysis in metaquomyoglobin. The dipolar shift as a structural probe. *J. Am. Chem. Soc.* **115**, 9754–9762 https://doi.org/10.1021/ja00074a049

42 Svistunenko, D.A., Sharpe, M.A., Nicholls, P., Blenkinsop, C., Davies, N.A., Dunne, J. et al. (2000) The pH dependence of naturally occurring low-spin forms of methaemoglobin and metmyoglobin: an EPR study. *Biochem. J.* **351**, 595–605 https://doi.org/10.1042/bj3510595

43 Romero, F.J., Ordonez, I., Arduini, A. and Cadenas, E. (1992) The reactivity of thiols and disulfides with different redox states of myoglobin. Redox and addition reactions and formation of thiyl radical intermediates. *J. Biol. Chem.* **267**, 1680–1688 https://doi.org/10.1016/S0021-9258(18)45999-6

44 Sono, M., Perera, R., Jin, S., Makris, T.M., Sligar, S.G., Bryson, T.A. et al. (2005) The influence of substrate on the spectral properties of oxyferrous wild-type and T252A cytochrome P450-CAM. *Arch. Biochem. Biophys.* **436**, 40–49 https://doi.org/10.1016/j.abb.2004.12.026

45 Kimmich, N., Das, A., Sevrioukova, I., Meharenna, Y., Sligar, S.G. and Poulos, T.L. (2007) Electron transfer between cytochrome P450cin and its FMN-containing redox partner, cindoxin. *J. Biol. Chem.* **282**, 27006–27011 https://doi.org/10.1074/jbc.M703790200

46 Ueno, T., Nishikawa, N., Moriyama, S., Adachi, S., Lee, K., Okamura, T.-A. et al. (1999) Role of the invariant peptide fragment forming NH⊙⊙⊙ S hydrogen bonds in the active site of cytochrome P-450 and chloroperoxidase: synthesis and properties of Cys-Containing peptide Fe (III) and Ga (III) (Octaethylporphinato) complexes as models. *Inorg. Chem.* **38**, 1199–1210 https://doi.org/10.1021/ic980710u

47 Hiner, A.N., Raven, E.L., Thorneley, R.N., Garcia-Canovas, F. and Rodriguez-Lopez, J.N. (2002) Mechanisms of compound I formation in heme peroxidases. *J. Inorg. Biochem.* **91**, 27–34 https://doi.org/10.1016/S0162-0134(02)00390-2

48 Moody, P.C.E. and Raven, E.L. (2018) The nature and reactivity of ferryl heme in compounds I and II. *Acc. Chem. Res.* **51**, 427–435 https://doi.org/10.1021/acs.accounts.7b00463

49 Rittle, J. and Green, M.T. (2010) Cytochrome P450 compound I: capture, characterization, and C-H bond activation kinetics. *Science* **330**, 933–937 https://doi.org/10.1126/science.1193478

50 Ozaki, S., Matsui, T. and Watanabe, Y. (1997) Conversion of myoglobin into a peroxygenase: a catalytic intermediate of sulfoxidation and epoxidation by the F43H/H64L mutant. *J. Am. Chem. Soc.* **119**, 6666–6667 https://doi.org/10.1021/ja970453c

51 Matsui, T., Ozaki, S. and Watanabe, Y. (1997) On the formation and reactivity of compound I of the His-64 myoglobin mutants. *J. Biol. Chem.* **272**, 32735–32738 https://doi.org/10.1074/jbc.272.52.32735

52 Re, R., Pellegrini, N., Proteggente, A., Pannala, A., Yang, M. and Rice-Evans, C. (1999) Antioxidant activity applying an improved ABTS radical cation decolorization assay. *Free Radic. Biol. Med.* **26**, 1231–1237 https://doi.org/10.1016/S0891-5849(98)00315-3

53 Ozaki, S. and Ishikawa, Y. (2006) One- and two-electron oxidation by the GLY-65 to threonine myoglobin mutant. *React. Kinet. Catal. L* **89**, 21–28 https://doi.org/10.1007/s11144-006-0082-7

54 Carlsen, C.U. and Skibsted, L.H. (2004) Myoglobin species with enhanced prooxidative activity is formed during mild proteolysis by pepsin. *J. Agric. Food Chem.* **52**, 1675–1681 https://doi.org/10.1021/jf030494u